A&A manuscript no.
(will be inserted by hand later)

Your thesaurus codes are:
07(02.08.1;02.09.1;08.03.1;08.03.4;08.13.2;08.16.4)

ASTRONOMY
AND
ASTROPHYSICS
20.12.1994

Circumstellar Dust Shells around Long-period Variables

III. Instability due to an exterior κ–mechanism caused by dust formation

A. J. Fleischer[1], A. Gauger[2], E. Sedlmayr[1]

[1] Technische Universität Berlin, Institut für Astronomie und Astrophysik, PN 8-1, Hardenbergstr. 36, D–10623 Berlin, Federal Republic of Germany
[2] Los Alamos National Laboratory, Group T–4, MS B268, Los Alamos, NM 87545, USA

Received ; accepted

Abstract. Dynamical models of circumstellar dust shells (CDS) around very luminous carbon–rich long-period variables are presented which include time-dependent hydrodynamics and a detailed treatment of the processes of formation, growth and evaporation of the dust grains. In contrast to our previous calculations, where we assumed that the sinusoidally moving inner boundary simulates the interior pulsation of the star, we now present model calculations, where the velocity of the inner boundary is equal to zero.

A new nonlinear effect arises because of the dust opacity: By the backwarming due to the formation of a discrete dust layer, small–amplitude waves are initiated in the innermost region which provide a density enhancement necessary for a new dust formation and growth cycle. It is shown how this mechanism starts in an initially hydrostatic atmosphere and how it is self-maintaining due to the induced waves. Hence, the circumstellar shell mimics a pulsating atmosphere, although this effect is caused by an instability due to the dust formation process.

Furthermore, it is shown that this modeling approach yields stationary dust–driven wind models as a limiting case. However, this is only achieved if the dust opacity is neglected in the determination of the temperature in radiative equilibrium or if dust formation is so ineffective that no relevant backwarming occurs.

Since very high luminosities and low temperatures are needed for the exterior κ–mechanism to occur by itself, the pure effect as described in this paper probably will not show up in general but only for objects at the very end of their AGB evolution. However, as AGB stars are usually pulsating objects, a complex interaction between the pulsation and the exterior κ–mechanism is likely to occur in a broader range of parameters.

Send offprint requests to: A. J. Fleischer
Internet: `fleischer@physik.TU-Berlin.DE`

Key words: hydrodynamics – instabilities – stars: carbon – circumstellar matter – stars: mass–loss – stars: AGB and post–AGB

1. Introduction

A characteristic feature of stars evolving along the Asymptotic Giant Branch (AGB) is the occurrence of pulsation accompanied by a substantial mass loss. Especially the phase of large–amplitude, long–period pulsations seems to be characterized by the most rapid mass loss. These long–period variables (LPVs) have a period range which scatters around a maximum by number of ≈ 350d (Hoffmeister et al. 1984, Olofsson et al. 1993a) and mass loss rates up 10^{-4} $M_\odot$ yr^{-1} (e.g. Knapp & Morris. 1985, Loup et al. 1993).

Time–dependent model calculations of circumstellar dust shells (CDS) around LPVs take the effects of pulsation into account by applying the so–called *piston* approximation (Wood 1979, Bowen 1988, Bowen & Willson 1991, Fleischer et al. 1992 (henceforth called Paper I), Feuchtinger et al. 1993). Thereby, the pulsation is described by a sinusoidally moving inner boundary of the model grid, which is situated a few percent in radius below the photosphere. In Paper I we presented dynamical models of CDS around carbon–rich LPVs which include for the first time a detailed treatment of dust formation, growth and evaporation and demonstrated clearly the key role of the dust complex for the resulting physical structure of the CDS. We found that the dust is strongly correlated to the hydrodynamical quantities, and that radiation pressure on dust is able to produce dominant strong shock waves which run through the atmosphere. In Winters et al.

(1994b, henceforth called Paper II) we investigated the optical appearance of these dust shell models and found that the dust complex also decisively influences the lightcurves of the objects under consideration.

The aforementioned investigations have in common, that pulsation together with radiation pressure on dust grains can account for the observed high mass loss rates of LPVs and Miras.

On the other hand, extensive work has been performed to construct time-independent or so–called *stationary* wind models of late type giants which include radiation pressure on dust as the only force for driving the outflow (e.g. Lucy 1976, Menietti & Fix 1978, Berruyer & Frisch 1983, Tielens 1983, Kozasa et al. 1984, Gail & Sedlmayr 1985). The self–consistent stationary wind models of Gail and Sedlmayr (1987a), Dominik et al. (1990), and Winters et al. (1994a) are completely determined by the prescription of the four fundamental parameters: stellar mass M$\star$, stellar luminosity L$\star$, effective temperature $T_\star$ and the chemical abundances ϵ_i. They showed that the mass loss rates and final outflow velocities resulting from their models for dust-enshrouded AGB objects are in good agreement with the observed range of values. The theoretical spectra calculated with this model approach closely match those of large, luminous, dusty carbon–stars, e.g. that of the prominent infrared object IRC +10216. An important result is, that purely dust–driven winds are possible only in a certain region of the HR–diagram (Gail & Sedlmayr 1987b, Dominik et al. 1990). Gail & Sedlmayr (1987b) deduced a minimum mass loss rate, for both the carbon–rich as well as for the oxygen-rich case, necessary to drive the circumstellar wind by radiation pressure on dust grains. Below this mass loss rate the wind cannot be driven by this mechanism alone.

With regard to these two different modeling approaches, time–dependent and stationary, we will address to the following questions. Whether and under which conditions is it possible with our dynamical code to obtain stellar wind models with a nonmoving inner boundary, i.e. is it possible to explore the regime of purely dust–driven outflows? Which conditions have to be satisfied to construct a "stationary wind" solution and which physical quantities limit the existence of such a solution, and if such a solution exists, is it stable?

It is demonstrated that a dust instability effect or exterior κ–mechanism causes atmospheric oscillations, and the stationary dust–driven wind solution is a limiting case of the physical problem. However, as very high luminosities and low temperatures are needed for the pure effect to occur by itself, we do not expect that the exterior κ–mechanism is a dominant mechanism for mass loss on the AGB. This mechanism alone probably will only show up during a rather short phase at the end of the AGB evolution. Before this final evolutionary stage, however, we expect that the complex interplay between the interior pulsation of the star and the exterior κ–mechanism is decisive for characteristic time scales of the CDS, e.g. determines when a new dust layer is formed. This leads to the effect of *multiperiodicity* which will be subject of a forthcoming paper. Exemplary multiperiodic models as well as corresponding lightcurves have been already presented in Paper II. The present paper merely introduces this new dust instability effect at the price that extreme model parameters have to be chosen in order to clearly demonstrate the implications of the mechanism.

We start with a short outline of our modeling method in Sect. 2. In Sect. 3 we present the results of our calculations. In Sect. 3.1 we investigate the physical conditions which are responsible for the onset of the instability in the initial phase of the model calculation. A self–maintaining driving mechanism for a massive outflow from cool luminous stars is presented in Sect. 3.2. The exterior κ–mechanism turns out to have an eigenperiod, which is discussed in Sect. 3.3. In Sect. 3.4 the limit luminosity for the onset of the κ–mechanism is discussed. The limit case of a stationary dust driven wind is presented in Sect. 3.5. Sect. 4 contains the results of a larger series of models, and thereby the dependence of the results on the fundamental model parameters is discussed. We finish this paper with some concluding remarks in Sect. 5.

2. The modeling method

Since the details of the modeling method and the basic equations have been discussed in Paper I, we only give a brief summary of the main ingredients.

We consider a spherically symmetric shell around a red giant with mass $M_\star$, effective temperature $T_\star$, and luminosity $L_\star$. Possible effects of rotation and magnetic fields are neglected. The time–dependent hydrodynamical equations are written in Lagrangian coordinates and solved by explicit integration according to the difference scheme given in Richtmyer & Morton (1967).

Usually, a constant gas opacity $\kappa_g = 2.0\,10^{-4}\mathrm{cm}^2\ \mathrm{g}^{-1}$ as in Paper I is used. Optionally, a variable gas opacity can be used. In this case the Rosseland mean value of κ_g is interpolated from tables kindly provided by M. Scholz (Scholz & Tsuji 1984). Radiative acceleration resulting from molecular opacities, as considered e.g. by Jørgensen & Johnson (1992), is not taken into account. Furthermore, post-shock cooling can be optionally taken into account by respective cooling functions in the gas energy equation. A LTE-approximation is then used to describe the source function. Otherwise, all thermodynamic processes are assumed isothermal.

The set of moment equations describing dust formation, growth and dust destruction due to thermal evaporation developed by Gail & Sedlmayr (1988) and Gauger et al. (1990) is solved simultaneously with the hydrodynamical equations. Effects of grain drift are not taken into account. For the calculation of the dust complex it is essential to know the chemical composition of the gas phase.

We use the same set of hydrocarbons (H, H_2, C, C_2, C_2H, C_2H_2) in chemical equilibrium as in Paper I to calculate the particle densities of the species contributing to the growth of carbon grains. Solar abundances (Allen 1973) are assumed for all elements except for the abundance of carbon ϵ_C which we consider as a free model parameter in order to account for a carbon–rich element composition. Grain nucleation is treated by means of classical nucleation theory. This approach has been critized (e.g. Donn & Nuth 1985, Cadwell et al. 1994, cf. also Sedlmayr 1994), however, lacking a more sufficient and numerically treatable description we rely on this approach.

The radiative transfer problem is treated by the semi–analytical method of Lucy (1971, 1976) which yields the local equilibrium temperature T_{eq} at every instant of time. In the limit case of isothermal shocks, where post–shock cooling occurs instantaneously, T_{eq} equals the gas temperature T_g throughout the atmosphere.

Since we do not take into account pulsation for the present calculations, our models are defined by the prescription of the 4 fundamental stellar parameters ($T_\star$, $L_\star$, $M_\star$, ϵ_i). To start the calculation an initially hydrostatic model with the selected number of grid points is constructed. The calculation of the dust complex is started in the initial model and the development of the model run is followed until a "cyclic" pattern of the radial structure or a stationary solution is reached.

3. Results

We want to deal with the problem in two steps. First we investigate the initial phase of a model run, i.e. the hydrostatic phase. As a second step we describe the mechanism which causes a self–maintaining outflow without additional energy input by the interior pulsation, i.e. by a piston.

In order to demonstrate clearly the effect extreme stellar parameters have to be chosen compared to classical optical Miras, cf. Tab. 1. Nevertheless, these values are appropriate for bright carbon stars (Jura 1991, Olofsson et al. 1993b) in particular with respect to luminosities and stellar temperatures.

3.1. The onset of the instability

Figure 1 shows the radial structure of different quantities for 4 hydrostatic models with different luminosities. The radius is given in units of $10^2 R_\odot$. The following quantities are plotted:

upper diagram: the temperature T (solid lines, l.h.s ordinate) and the supersaturation ratio S as defined below (dashed lines, r.h.s ordinate),

lower diagram: the logarithm of the density ρ (solid lines, l.h.s. ordinate) and the logarithm of the nucleation rate $J_\star$ (dashed lines, r.h.s ordinate), i.e. the number of grains formed from the gas phase per second and per H–atom.

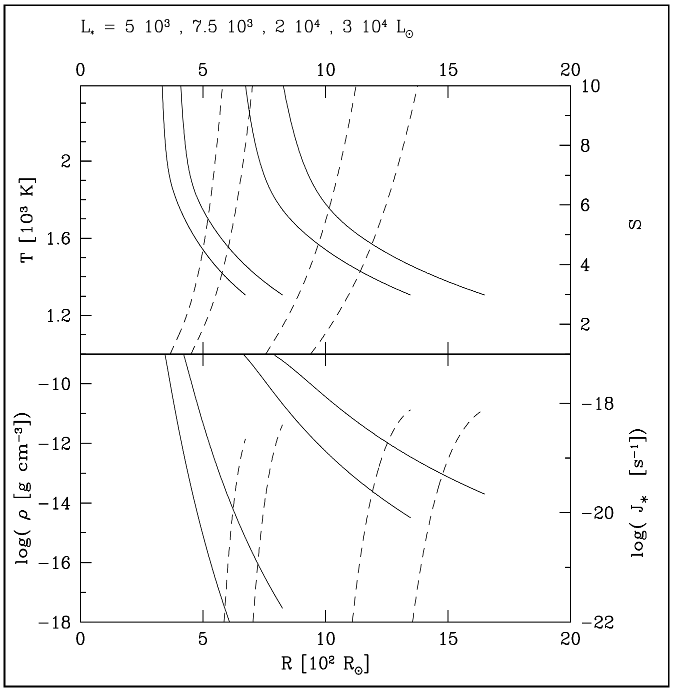

Fig. 1. Radial course of temperature (solid lines), supersaturation ratio (dashed lines), density (solid lines), and nucleation rate (dashed lines) of initial hydrostatic models with $M_\star = 1.0$ $M_\odot$, $T_\star = 2600$ K, $\epsilon_C/\epsilon_O = 1.80$, and different luminosities $L_\star$. The luminosity increases from left to right, i.e. the higher the luminosity, the more extended is the model. Note that the radius is given in units of the solar radius

From left to right the curves belong to the models with $L_\star = 5.0\,10^3, 7.5\,10^3, 2.0\,10^4, 3.0\,10^4 L_\odot$, respectively. An overabundance of carbon to oxygen $\epsilon_C/\epsilon_O = 1.80$ is chosen to provide sufficient condensable material.

Our modeling approach includes the description of the formation of small clusters from the gas phase by means of the classical nucleation theory, i.e. the formation of clusters of a critical size in a supersaturated vapor is described by means of thermodynamical quantities. The supersaturation ratio S is defined by

$$S = \frac{p(1)}{p_v(1)} \quad , \tag{1}$$

where $p(1)$ denotes the partial pressure of monomers of the condensing species and $p_v(1)$ denotes the vapor saturation pressure with respect to the dust temperature which equals T_{eq}. The quantity S determines whether dust formation starts: if S is below 1 no dust condenses. However, the real onset of nucleation requires not only $S \geq 1$ but S has to exceed a minimum supersaturation ratio S_c. We adopt a value of $S_c = 3$ (cf. Draine & Salpeter 1977) to start the dust calculation in a given Lagrangian zone.

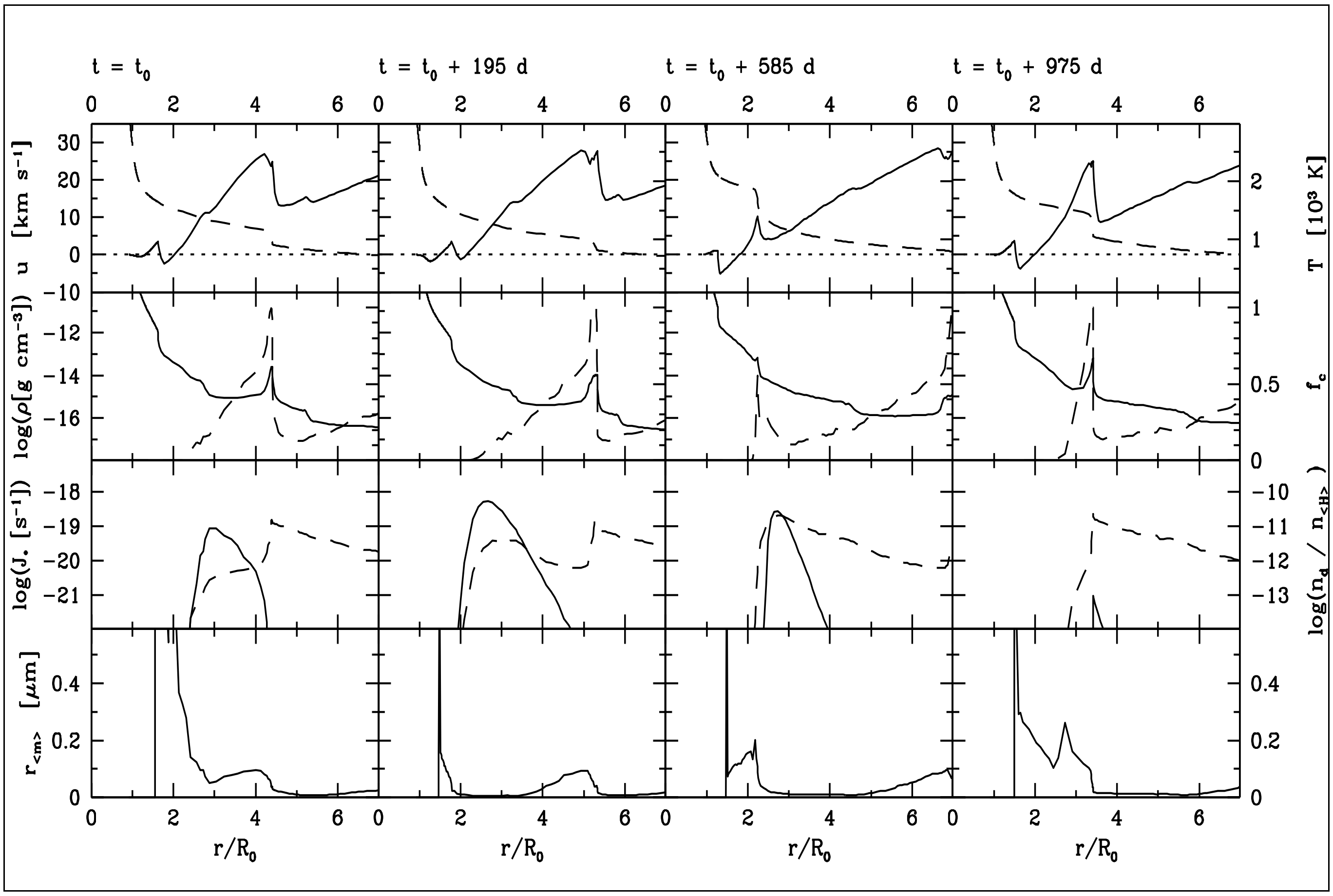

Fig. 2. Radial structure of characteristic hydrodynamical quantities, and quantities describing the dust of a model where the dust opacity *is* taken into account in the determination of the radiative equilibrium temperature. The quantities are explained in detail in the text. The model is *not* driven by a piston. The model parameters are: $M_\star = 1.0\ M_\odot$, $T_\star = 2600$ K, $L_\star = 2.0\ 10^4\ L_\odot$, $\epsilon_C/\epsilon_O = 1.80$, which is Model No. 2 of Tabs. 1 and 2.

From Fig. 1 we infer that dust formation is possible in all four hydrostatic initial models, since the value of $S_c = 3$ is exceeded in all models. The nucleation rates reach equally high values, but the curves cover a rather narrow spatial region for the first two models on the left, whereas a broad peak does occur for the high–luminosity models on the right. However, only in the latter two models does nucleation occur in a dense environment, whereas in the models with $L_\star = 5.0\ 10^3$ and $7.5\ 10^3\ L_\odot$ the density is almost four orders of magnitude smaller. This allows an effective growth phase of the newly formed critical clusters in the high–luminosity models and a subsequent development of an outflow driven by radiation pressure acting on the newly formed dust grains even without additional input of mechanical energy. In both of the low–luminosity models the onset of this instability is prevented since almost no dust growth is possible, hence, almost no radiation pressure on dust results, and thus, no outflow is initiated.

Note that S and $J_\star$ also depend on ϵ_C/ϵ_O, hence, sufficiently high values of ϵ_C/ϵ_O could ensure the onset of the instability. However, also the opposite is true. Low values of the overabundance of carbon could prevent the onset of the instability even in high–luminosity models.

Qualitatively, the situation is the same for the initial models with a variable gas opacity κ_g. However, due to the variable κ_g different density structures arise, which run parallel to the structures of the models above, but at densities up to two orders of magnitude lower. Thus, dust formation starts less effectively and a quantitative change occurs with respect to the value of the luminosity at which the instability appears.

To summarize in general: *the onset of the instability, i.e. the occurrence of substantial dust formation in an initially hydrostatic model, and the development of an outflow is determined by the density gradient of the model. The higher the luminosity, the more extended is the initial model and the larger is the static scale height. Hence, the two high–luminosity models of Fig. 1 show the de-*

velopment of an instability, solely caused by dust formation. Dust formation which occurs in the outer layers of these two models might be a single event during the initial model run. We have to follow the further development of the calculation to investigate whether dust formation is continuously possible, and thus, whether it yields a permanent driving mechanism for the wind. This is done in the following section.

3.2. Instability due to an exterior κ–mechanism

Figure 2 shows a sequence of the radial structure of the CDS at four successive instants of time of an exemplary model calculation. Note that from now on, the radius is given in units of the stellar radius of the initial hydrostatic model. Since only the dust forming region is of interest here, we have plotted only the innermost part of the CDS.

In Fig. 2 the following quantities are plotted:

upper row: the velocity u (solid lines, l.h.s. ordinate), dotted zero velocity line for comparison, and the temperature T (dashed lines, r.h.s. ordinate),

2nd row: the logarithm of the density ρ (solid lines, l.h.s. ordinate), and the degree of condensation f_c (dashed lines, r.h.s. ordinate), i.e the fraction of condensable material actually condensed into grains,

3rd row: the logarithm of the nucleation rate $J_\star$ (solid lines, l.h.s. ordinate) and the logarithm of the number of dust grains per H–atom $n_d/n_{<H>}$ (dashed lines, r.h.s. ordinate),

lower row: the mean particle radius $\mathrm{r}_{<m>}$ (solid lines).

Although Fig. 2 shows a sequence of the evolved model with $\mathrm{L}_\star = 2.0\ 10^4\ \mathrm{L}_\odot$ the instant of time t_0 could be conceived to be shortly after the initial phase. The first dust shell has formed as described in the previous section, and is now located at 4.2 $\mathrm{R}_\star$. This dust layer induced the corresponding shock wave by the process described in detail in Paper I.

By the substantial backwarming effect caused by the innermost dust layer the temperature in the wake of the shock front is increased. The increase of the temperature amounts to values of 100 K in the region around the stellar radius. Consequently, this leads to a slight increase of the pressure in the innermost region, and a subsequent generation of small–amplitude waves in the region below the stellar radius. These subsonic disturbances steepen due to the density gradient in the innermost region, and develop into wave fronts with amplitudes of $\approx$ 1 $\mathrm{km\,s^{-1}}$. Such a wave front can be seen at $\approx$ 2 $\mathrm{R}_\star$ in the velocity plot of Fig. 2 at $t = t_0 + 195d$. These newly generated wave fronts run outwards and finally compress the grain-bearing material at $\approx 2\ \mathrm{R}_\star$, thereby triggering dust growth. The grain nuclei are formed in the wake of the previous fully developed shock wave, where effective nucleation takes place, cf. the broad peak of the nucleation rate at $t = t_0 + 195d$, and the corresponding small mean particle radius in this region. Subsequently, effective dust growth follows due to the compression by the waves, and at $t = t_0 + 585d$ already a degree of condensation of 0.6 at $\approx 2.3 R_\star$ is reached. At this instant of time it can also be seen that substantial backwarming causes a noticeable step in the temperature structure, thereby starting the next cycle of wave formation.

In the following, at radii around 3.3 $\mathrm{R}_\star$, the grains grow very effectively and at $t = t_0 + 975\mathrm{d}$ a degree of condensation of almost 1.0 is reached. Radiation pressure acts on the newly formed grains and via the close momentum coupling between grains and gas the whole two–component medium is accelerated to supersonic velocities. A new shock front forms which sweeps up the material and again enhances the conditions for dust growth. Nucleation of grains dies off in the wake of the newly formed shock front since the temperature becomes too high by the backwarming of the newly developing dust shell. Finally, at $t = t_0 + 975\mathrm{d}$, the nucleation rate $J_\star$ almost completely vanishes since all condensable material in the shock front is actually condensed into grains and a broad new dust shell is formed.

During this phase the small–amplitude waves in the innermost region of the CDS run into a gas which is free of newly formed dust particles and therefore without causing any effect on the dynamics these waves are rapidly damped. When finally the new dust layer has moved farther outwards and the temperature drops below $\approx$ 1300K a new nucleation phase starts and the whole process starts again.

The radial course of the mean particle radius shows that at $t = t_0$ and $t = t_0 + 975d$ rather large particles (up to 2 μm) are present in a broader region around 2 $\mathrm{R}_\star$. However, these are only very few particles as can be seen by the number of dust grains per H–atoms $n_d/n_{<H>}$, which equals almost zero in this radius interval. During phases of effective dust nucleation ($t = t_0 + 195d$ and $t = t_0 + 585d$) $n_d/n_{<H>}$ is substantially decreased, and most of the particles are accelerated outwards, whereas only a few large grains remain at the inner edge of the dust shell as can be seen from the narrow peak of $r_{<m>}$ at 1.7 $\mathrm{R}_\star$ at $t = t_0 + 195d$ and $t = t_0 + 585d$. The radial course of the mean particle radius indicates that the large majority of dust particles is small compared to the relevant wavelengths of the radiation field.

Additionally, we have plotted in Fig. 3 the radial structure of the geometrically diluted optical depth τ_L, cf. Lucy (1971), and of the monochromatic optical depth $\tau_{1\mu\mathrm{m}}$ for the same instants of time shown in Fig. 2. We assume that the dust particles are small compared to the wavelength, and we use the complex refractive index of amorphous carbon at 1μm as given in Maron (1990). The quantities $\tau_{1\mu\mathrm{m}}$ and τ_L are measured inwards adopting the boundary condition $\tau_{1\mu\mathrm{m}}(\infty) = \tau_L(\infty) = 0$.

The plot shows that at $t = t_0$ and $t = t_0 + 195d$ the monochromatic optical depth in the innermost region is mostly determined by the dust layer formed in the previ-

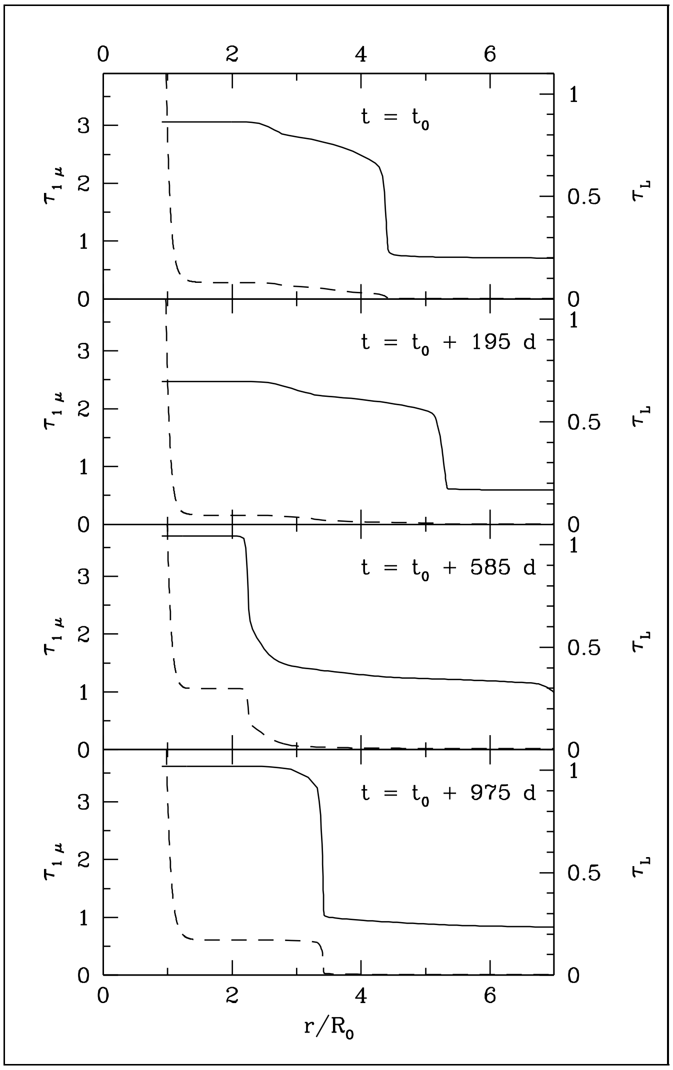

Fig. 3. Radial structure of the monochromatic optical depth τ at $\lambda = 1\mu$m (solid line, l.h.s. ordinate) and of the geometrically diluted optical depth τ_L (dashed line, r.h.s. ordinate) for Model No. 2 at the same instants of time as in Fig. 2

ous cycle which is now moving outwards. At the following instants of time the newly formed dust layer determines the optical depths in the innermost region.

Summarizing, *we find, that even in models without interior pulsation, the dust complex is able to build up a self-maintaining mechanism which produces an outflow which is periodically traversed by strong shock waves. However, there are essentially two prerequisites necessary for this mechanism:*

1. The scale height of the initial hydrostatic model must be low enough to allow for dust formation already in this initial phase.
2. The interaction between the dust complex and the thermodynamics, i.e. the backwarming which raises the temperature, is necessary to initiate pressure–driven waves.
3. The backwarming of a preceding dust layer determines also when and where new dust particles are formed. Thus, this instability mechanism is self–regulated.

In these models the action of the dust complex is twofold. First, it initiates small–amplitude waves, which compress the material in the dust forming region, necessary for effective growth in the following cycle. Second, by the existence of the dust grains radiative momentum is transmitted to the wind, and dust drives the massive outflow.

Since backwarming due to the dust opacity in the CDS plays the key role for this process we call this mechanism *exterior κ–mechanism.*

A similar mechanism of instability is known from the line–driven winds of hot luminous stars (e.g. Rybicki 1987, Owocki et al. 1988, Owocki 1990). In this context, small-scale fluctuations of the radial outflow velocity cause a Doppler-shift of the local line-frequency out of the shadow of the surrounding material, which results in an increased line–force which subsequently tends to increase the flow velocity. An instability analysis (for a review see e.g. Rybicki 1987) shows that these perturbations have rather large growth rates, such that they quickly become nonlinear, and small initial perturbations suffice to result in a wind traversed by shock waves.

3.3. The eigenperiod

We have shown in the previous section that the exterior κ–mechanism produces strong shock waves which are caused by self–regulated formation of dust particles. Following the development of the model a little further than shown in Fig. 2 reveals, that the exterior κ–mechanism is a *periodic* phenomenon. The analysis of the model plotted in Fig. 2 shows that a shock develops once each 1105d. This time scale is the characteristic or *eigenperiod* of the CDS, which is inherent to the dust–forming system. The CDS quickly adjusts to that eigenperiod after the beginning of the model run, and remains stable till the end of the model calculation. A typical model run covers up to 15 cycles of the eigenperiod. As discussed in Sect. 4 the characteristic period sensitively depends on the fundamental stellar parameters.

Since the system has an eigenperiod the question arises how is the interaction with an exterior mechanical force, namely the piston at the inner boundary, which so far has been kept non–moving.

Figure 4 depicts the radial structure of the same quantities as in Fig. 2 for a model with the same stellar parameters, but now the model is driven by a piston with a period of 650d and an amplitude of 2 km s^{-1}. As indicated, two instants of time are plotted on top of each other.

Figure 4 shows that, although a piston is applied at the inner boundary, the additional energy and the period of this external force has almost no influence on the timescale of the circumstellar shell. In the outer parts, i.e. above 3

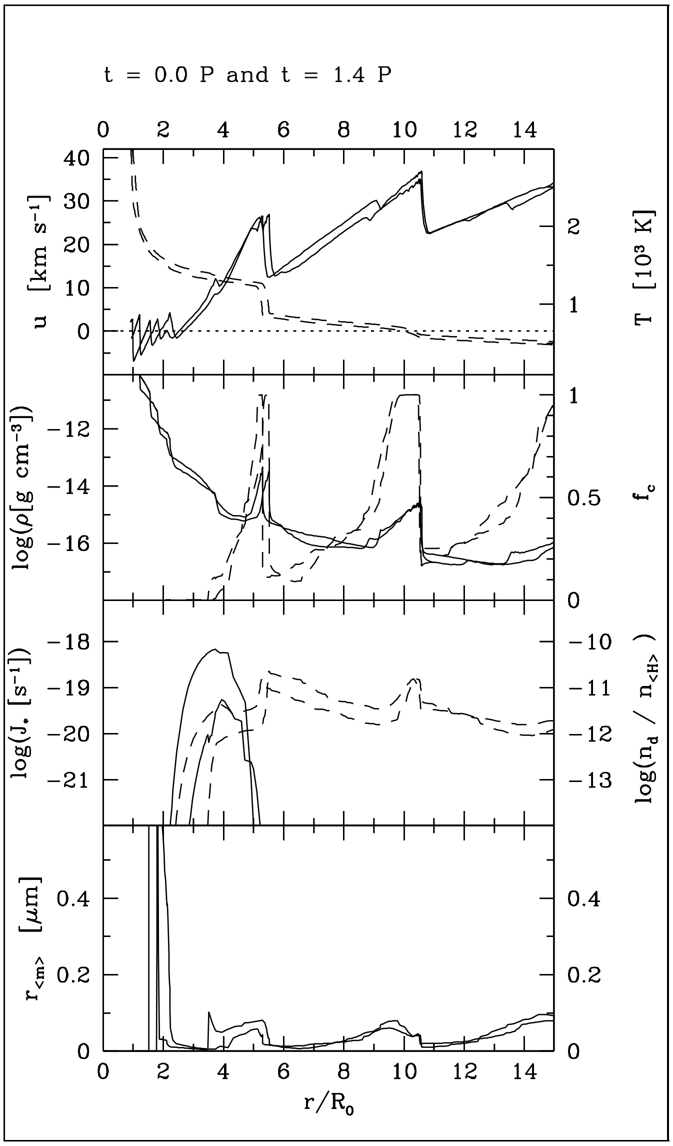

Fig. 4. Radial structure of the same quantities as in Fig. 2 of Model No. 19, cf. Tabs. 1 and 2, at two different instants of time. The dust opacity *is* taken into account in the determination of the radiative equilibrium temperature *and* the model is driven by a piston with period 650d and an amplitude of 2 km s^{-1}. The plot demonstrates the independence of the CDS of the interior pulsation for this set of model parameters.

$R_\star$, the shell exhibits a cyclic pattern on a scale of 910d which is only little below the eigenperiod of 1105d determined for the case without piston. The outer parts of the CDS behave almost independently from the time scale introduced by the piston. For models with an even higher luminosity, e.g. 3 10^4 $L_\odot$, the CDS oscillates exactly on its eigenperiod even if driven by a piston. In any case, the inner parts, i.e. here below 3 $R_\star$, are completely dominated by the influence of the piston. At the instants of time shown, the courses of the velocity and the density in this innermost region are almost 180° phase-shifted, since these instants of time belong to the beginning and approximately to the middle of the *pulsational* period provided by the piston.

That the eigenperiod of the model presented here (with $L_\star$ = 2.0 10^4 $L_\odot$) equals that of Model No. 1 in Tab. 1 with $L_\star$ = 3.0 10^4 $L_\odot$ stems from the fact that the influence of the piston causes an increase of the mean stellar radius during the model run, and hence, causes an increased mean luminosity.

We find that the dynamics of the CDS is dominated by different "driving–regimes": Among other calculations, Wood (1979) and Bowen (1988) also presented models which were purely driven by pulsation. These models represent one end of the scale of driving regimes, however, they can not account for the observed mass loss rates of LPVs. In Paper I we investigated the combined effect of pulsation and radiation pressure on dust. The model parameters of these calculations lie within the range where a dust–driven outflow is only possible with additional energy support. Most of the models presented in the present paper, are dominated by radiation pressure on dust. They represent the other end of the scale of driving regimes: purely dust–driven winds. The conditions for this regime are only met at the very end of the AGB evolution. If the stellar luminosity of these models is reduced, the dominance of the dust diminishes. Further reduction eventually leads to a vanishing outflow, if no additional energy support, e.g. by pulsation, accoustic waves (Pijpers 1994) or radiation pressure on molecules (Jørgensen & Johnson 1992), is provided.

3.4. The limiting luminosity for purely dust–driven outflows

To determine the limiting luminosity below which no dust–driven outflow is possible we have calculated a series of models with decreasing luminosity, while keeping the other parameters constant. The initial parameters as well as the resultant quantities are listed in Tabs. 1 and 2, respectively.

A first result evident from these tables is that the decrease of the radiative force causes reduced mass loss rates and substantially decreased final outflow velocities.

Figure 5 shows the radial structure of two models at the lower end of the luminosity scale. The same quantities as in Fig. 2 are plotted. To the upper row of the diagram we have added the course of the escape velocity u_{esc}, which is shown by the long-dashed line. In both of the models the dust opacity is taken into account for the determination of the radiative equilibrium temperature.

For the set of model parameters chosen, the transition from the range where the exterior κ–mechanism occurs to the range where the dust opacity can not influence the dynamics decisively, lies between $L_\star$ = 1.3 10^4 and 1.4 10^4 $L_\odot$. Although dust nucleation in both models is almost identical (cf. plot of $J_\star$ in Fig. 5), the slightly less

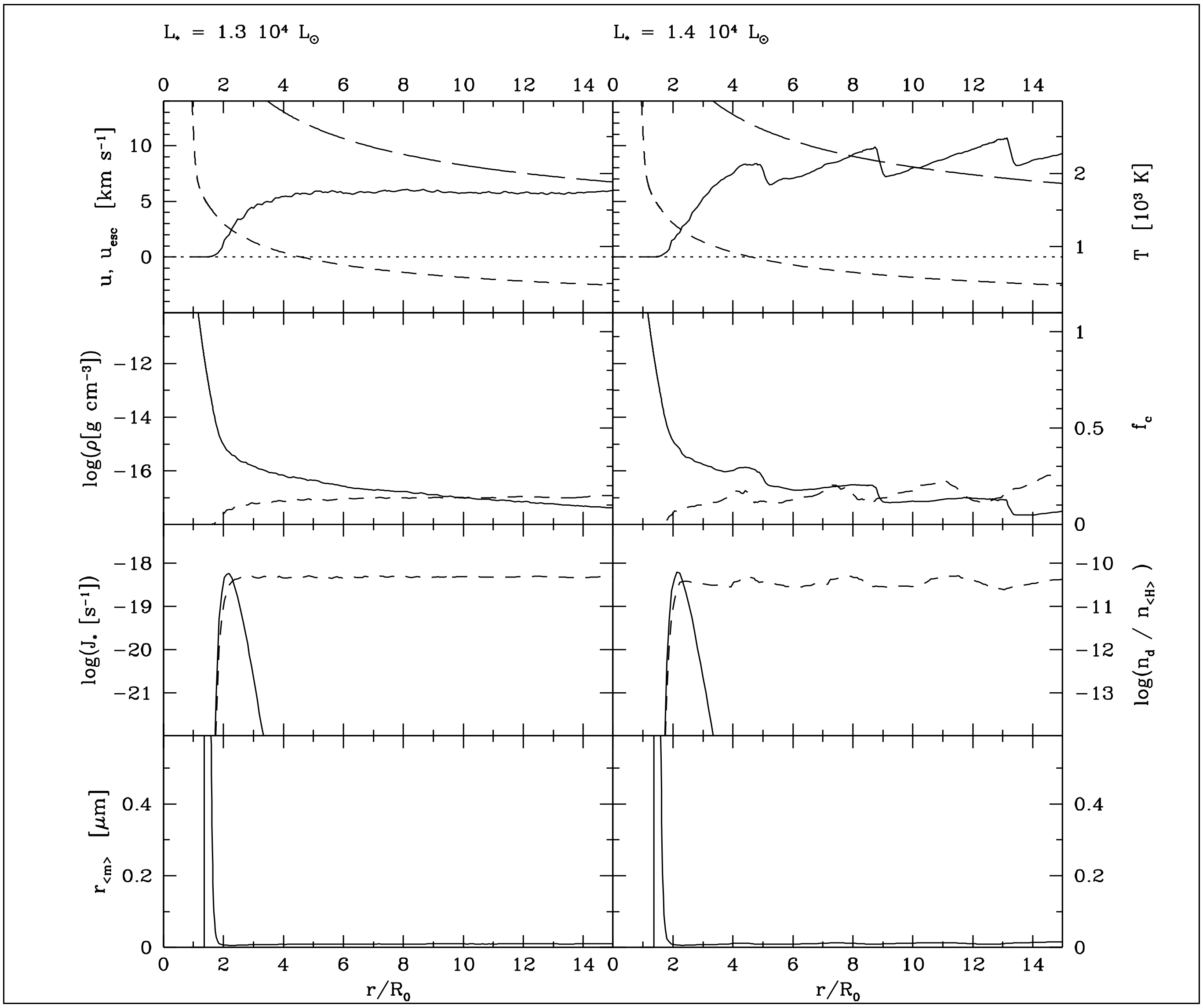

Fig. 5. Radial structure of two models with luminosities below and above the limiting luminosity for the occurrence of the exterior κ–mechanism. The parameters are equal to the model of Fig. 2 except for the luminosities which are $L_\star = 1.3\ 10^4\ L_\odot$ (l.h.s.) and $1.4\ 10^4\ L_\odot$ (r.h.s.), respectively, cf. also Tabs. 1 and 2. In *both* models the dust opacity *is* taken into account in the determination of the temperature in radiative equilibrium

steep density gradient of the r.h.s. model allows more effective dust growth, and hence, the exterior κ–mechanism is initiated.

This limiting luminosity also marks the dividing line below which no purely dust–driven outflow is possible. For the model with $L_\star = 1.30\ 10^4\ L_\odot$ radiation pressure on dust grains indeed is able to accelerate the flow to supersonic velocities, and the radiative force is even capable of accelerating the material to velocities above the escape velocity u_{esc} at a large distance form the star. However for lower luminosities the radiative force does not suffice to accelerate the material above u_{esc}. Below $1.30\ 10^4\ L_\odot$ a supersonic flow might develop for a time but will eventually collapse during the subsequent course of the model calculation.

As a general result, it should be noted that for values of the luminosity chosen around the limiting luminosity the radial structure of the model closely resembles that of a stationary dust–driven wind, compare the l.h.s. model of Fig 5, and the model calculations in e.g. Gail & Sedlmayr (1987a). Of course, the value of the limiting luminosity is different if other stellar parameters are chosen. A lower stellar temperature would shift the limiting luminosity towards lower values than for the model shown here. Thus, for each set of stellar parameters the limiting luminosity has to be separately determined (cf. also Sedlmayr & Dominik 1994).

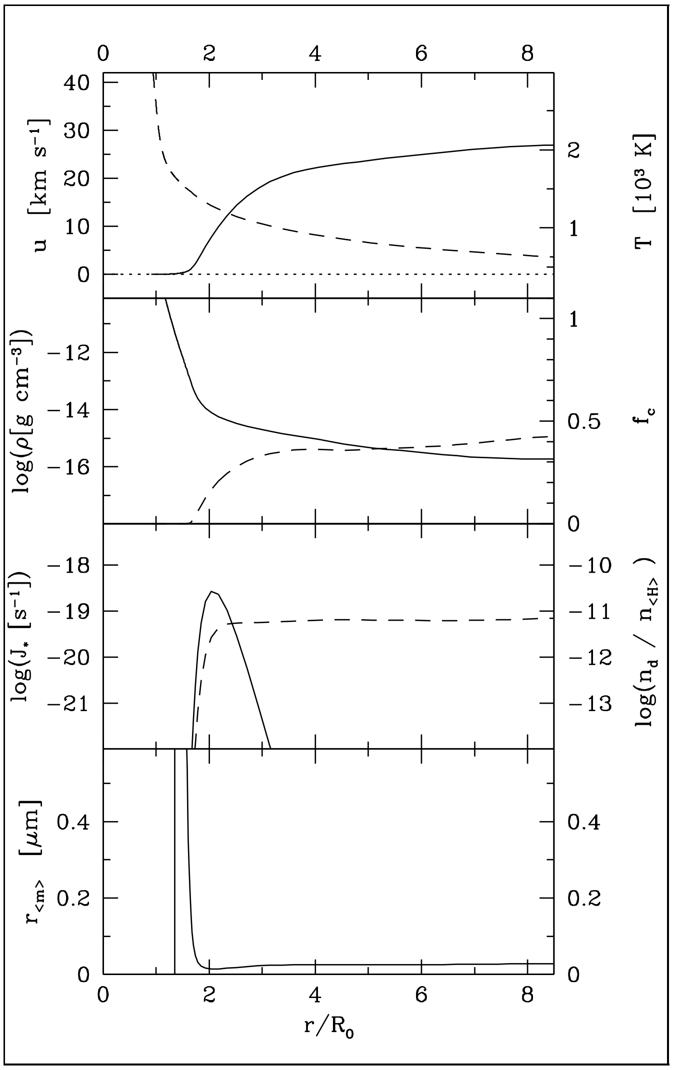

Fig. 6. Radial structure of characteristic hydrodynamical quantities and quantities describing the dust for a model where the dust opacity *is not* taken into account in the determination of the radiative equilibrium temperature, and the luminosity *is above* the limiting luminosity. The model parameters are the same as in Fig. 2: $M_\star = 1.0\ M_\odot$, $T_\star = 2600$ K, $L_\star = 2.0\ 10^4\ L_\odot$, $\epsilon_C/\epsilon_O = 1.80$. The model *is not* driven by a piston

3.5. The limiting case of a stationary dust–driven wind

We have shown that the dust opacity plays a key role in determining the dynamics of the CDS. In this section we investigate the case where the coupling between the dust complex and the thermodynamics is neglected, i.e. the case where only the constant gas opacity is taken into account for the determination of the temperature in radiative equilibrium.

Figure 6 shows the same quantities as Fig. 2 for a model calculation with exactly the same model parameters except that the temperature in radiative equilibrium is determined *without* taking into account the dust opacity. It should be noted that the value of the luminosity lies above the value of the limiting luminosity discussed in the preceding section.

The result is the typical radial structure of a stationary dust–driven wind around a carbon star (cf. e.g. the corresponding plots in Gail & Sedlmayr 1987a, Winters et al. 1994a). In the inner region, i.e. for radii below 1.5 $R_\star$, the dust–driven wind solution starts with low velocities of only a few meters per second. Only a small number of dust grains are present in this region, which due to the low velocities stay rather long in this innermost dense region. Therefore, they have excellent growth conditions and reach particle radii of a few μm, which despite possible further growth processes in the interstellar medium is consistent with radii determined for interstellar grains (Anders & Zinner 1993, Ott 1993). Since the nucleation rate is at least 8 orders of magnitude smaller in this innermost region than the relevant range shown in Fig. 6, there is only a tiny amount of these large particles, and the degree of condensation reached in this region is less than 10^{-6}.

The temperature decreases with increasing distance from the star. At $\approx 1.6\ R_\star$ radiation pressure on dust accelerates the flow to supersonic velocities. Around 2 $R_\star$ the temperature is sufficiently low such that the nucleation rate reaches its maximum value. Subsequently, these newly formed grains grow effectively and the degree of condensation increases.

In the outer region the nucleation rate rapidly decreases but the existing particles still grow, which leads to a continued increase of the degree of condensation. Finally, in this model $\approx 40\%$ of the condensable material is condensed into dust grains and a terminal velocity of ≈ 28 km s^{-1} is reached.

One main conclusion we draw from this surprising result is that the exterior κ–mechanism is indeed based on a physical process whose central component is the dust opacity. If numerical artifacts were responsible for the occurrence of the exterior κ–mechanism, the neglect of a physical interaction would have led to anything but a known, well–studied solution. Furthermore, the exterior κ–mechanism is confirmed by Höfner et al. (1994a) by means of a completely different numerical method.

The second conclusion concerns the stability of stationary dust–driven winds. Therefore it is again interesting to draw an analogy to the winds from hot, luminous stars. In his review Owocki (1990) quotes several arguments from observations as well as from theory that give reason to believe that the winds from hot stars are not stationary outflows but have an internal structure and a time variability. We have demonstrated, that there also exist stationary dust driven wind solutions for outflows from cool stars which are not stable if all interactions are taken into account in the time–dependent model calculation, since these models develop instabilities as shown in Sect. 3.2. In Sect. 3.4 we demonstrated that a stationary dust–driven wind solution results if the influence of the dust on thermodynamics becomes negligible due to suitably chosen model parameters. At present, we can only conjecture that instability is a general property of stationary dust–driven wind solutions if there are relevant amounts of dust. A proof of this conjecture, which clearly cannot be done by model calculations alone will be an interesting topic of future research but is beyond the scope of the present paper.

Thus, this and the preceding section may be summarized as follows: *we get the result that our code reproduces the stationary dust–driven wind solution for all parameters well above the limit for pure dust–driven winds if the coupling between the thermodynamics and the dust complex is neglected, and near the limiting luminosity if the coupling is taken into account.*

4. Discussion

In Tabs. 1 and 2 we have summarized the results of a grid of model calculations. These tables demonstrate the influence of the model parameters as well as the influence of modeling approximations on the exterior κ–mechanism.

4.1. Influence of the stellar luminosity

The first six models in Tabs. 1 and 2 represent a series of models with decreasing stellar luminosity. For $L_\star \leq 2.5\ 10^4\ L_\odot$ the eigenperiod increases with decreasing luminosity. However, the eigenperiod increases also for luminosities $> 2.5\ 10^4\ L_\odot$, i.e. longer eigenperiods are found for models with extraordinary high luminosities (e.g. $3\ 10^4\ L_\odot$ Model No. 1), and at the lower end of the luminosity scale (e.g. Model No. 5). Around an initial luminosity of $L_\star = 2.5\ 10^4\ L_\odot$ seems to be a minimum of the eigenperiod–luminosity correlation. In the high–luminosity models a dramatic backwarming occurs with a temperature increase in the inner region up to a few hundred K due to the effective dust formation process. Therefore, it takes a longer time interval till the temperature in the dust nucleation region has appropriately decreased to allow for the next dust nucleation cycle. The length of the eigenperiod also increases towards the limit luminosity of the exterior κ–mechanism. These models are characterized by a less effective dust formation process. The resulting self–induced shock waves therefore have a smaller amplitude and travel through the atmosphere at a much lower velocity. Thus, it takes longer till the radial pattern repeats itself. Between these two limiting cases there exists a configuration where the effects of backwarming and dust formation are in an optimum state, which yields a higher mass loss rate for Model No. 2 at a lower outflow velocity compared to Models No. 1 or No. 3.

4.2. Influence of the carbon overabundance

Model No. 3 and Models No. 7–10 represent a series of models with decreasing overabundance of carbon to oxygen. The values of ϵ_C/ϵ_O are chosen to accont for objects substantially enshrouded by dust. Thus, the values lie in the upper range of values found by abundance determinations (Lambert et al. 1986, Olofsson et al. 1993b). The luminosity of these models is well above the limiting luminosity for the exterior κ–mechanism, which is described in Sect. 3.4 for this set of parameters. The result is an inverse correlation between ϵ_C/ϵ_O and the eigenperiod of the atmosphere. An increase of the amount of condensable material, i.e. the ϵ_C/ϵ_O–ratio, results in a shortening of the eigenperiod, a result that is certainly to be expected: since the initial conditions were equal for the models of this series, a larger amount of condensable material ensures a higher reoccurrence frequency of the exterior κ–mechanism. The value of $\epsilon_C/\epsilon_O = 1.4$ causes a dramatic prolongation of the eigenperiod. Finally, below a value $\epsilon_C/\epsilon_O = 1.4$ no outflow is initiated (Model No. 10).

However, note that the mass loss rates of Models No. 3, 7 and 8 do not differ very much despite a reduction in ϵ_C/ϵ_O. For Model No. 7 $\dot{M}$ is even a little bit higher. For lower ϵ_C/ϵ_O–ratios (Models No. 9 and 10) a steep decrease of $\dot{M}$ is found, and a sharp ϵ_C/ϵ_O limiting value exists below which no outflow is possible at all. The outflow velocities are directly correlated with the ϵ_C/ϵ_O ratio. These correlations between $\dot{M}$, u_∞ and ϵ_C/ϵ_O are found for a broad range of model parameters, as well as for stationary models (Winters et al. 1994a) and also for models driven by a piston. They are investigated in detail in a forthcoming paper.

4.3. Influence of the stellar temperature

Model No. 3 and Models No. 11 – 13 represent a series of models with varying stellar temperature. Due to its lower temperature Model No. 11 provides more favourable conditions for dust growth compared to Model No. 3, which yields a reduced eigenperiod of Model No. 11. Increasing the stellar temperature yields a steep prolongation of the eigenperiod. Note that Model No. 13 is calculated with an increased luminosity to achieve an outflow which, nevertheless, has an unrealistic low mass loss rate. We conclude, that the exterior κ–mechanism alone can drive the wind only for cool objects. However, the temperatures needed for the exterior κ–mechanism to occur by itself are within the range observed for bright carbon stars: Only 8 objects of 75 sources listed in Tab. 3 of Olofsson et al. (1993b) have stellar temperatures equal or higher than 3000K.

Table 1. Parameter of the initial hydrostatic models: stellar luminosity $L_\star$, carbon overabundance ϵ_C/ϵ_O, stellar temperature $T_\star$, and stellar mass $M_\star$. Additionally given are quantities resulting from these initial models: stellar radius $R_\star$, density at the photosphere $\rho(R_\star)$, surface gravity $g(R_\star)$, and static scale height H_0

	$L_\star[10^4\ L_\odot]$	ϵ_C/ϵ_O	$T_\star$ [K]	$M_\star[M_\odot]$	$R_\star$ [$R_\odot$]	$\rho(R_\star)$ [g cm^{-3}]	$g(R_\star)$ [cm s^{-2}]	$H_0/R_\star$	Remarks
1	3.00	1.80	2600	1.0	852	$7.7\ 10^{-10}$	$3.8\ 10^{-2}$	$7.6\ 10^{-2}$	
2	2.50	1.80	2600	1.0	778	$9.2\ 10^{-10}$	$4.5\ 10^{-2}$	$7.0\ 10^{-2}$	
3	2.00	1.80	2600	1.0	696	$1.1\ 10^{-9}$	$5.7\ 10^{-2}$	$6.3\ 10^{-2}$	
4	1.50	1.80	2600	1.0	602	$1.5\ 10^{-9}$	$7.5\ 10^{-2}$	$5.4\ 10^{-2}$	
5	1.40	1.80	2600	1.0	582	$1.6\ 10^{-9}$	$8.1\ 10^{-2}$	$5.2\ 10^{-2}$	
6	1.30	1.80	2600	1.0	561	$1.7\ 10^{-9}$	$8.7\ 10^{-2}$	$5.0\ 10^{-2}$	
7	2.00	1.60	2600	1.0	696	$1.1\ 10^{-9}$	$5.7\ 10^{-2}$	$6.3\ 10^{-2}$	
8	2.00	1.50	2600	1.0	696	$1.1\ 10^{-9}$	$5.7\ 10^{-2}$	$6.3\ 10^{-2}$	
9	2.00	1.40	2600	1.0	696	$1.1\ 10^{-9}$	$5.7\ 10^{-2}$	$6.3\ 10^{-2}$	
10	2.00	1.30	2600	1.0	696	$1.1\ 10^{-9}$	$5.7\ 10^{-2}$	$6.3\ 10^{-2}$	
11	2.00	1.80	2500	1.0	752	$1.0\ 10^{-9}$	$4.8\ 10^{-2}$	$6.5\ 10^{-2}$	
12	2.00	1.80	2800	1.0	600	$1.4\ 10^{-9}$	$7.6\ 10^{-2}$	$5.8\ 10^{-2}$	
13	2.80	1.80	3000	1.0	618	$1.7\ 10^{-9}$	$11.4\ 10^{-2}$	$4.0\ 10^{-2}$	
14	2.00	1.80	2600	0.9	696	$1.0\ 10^{-9}$	$5.1\ 10^{-2}$	$7.0\ 10^{-2}$	
15	2.00	1.80	2600	1.3	696	$1.7\ 10^{-9}$	$7.4\ 10^{-2}$	$4.8\ 10^{-2}$	
16	2.00	1.80	2600	1.6	696	$2.0\ 10^{-9}$	$9.1\ 10^{-2}$	$3.9\ 10^{-2}$	
17	2.00	1.80	2600	1.0	696	$1.1\ 10^{-9}$	$5.7\ 10^{-2}$	$6.3\ 10^{-2}$	without κ_d
18	2.00	1.80	2600	1.0	696	$1.1\ 10^{-9}$	$5.7\ 10^{-2}$	$6.3\ 10^{-2}$	without κ_d, piston
19	2.00	1.80	2600	1.0	696	$1.1\ 10^{-9}$	$5.7\ 10^{-2}$	$6.3\ 10^{-2}$	piston
20	2.00	1.80	2600	1.0	696	$1.1\ 10^{-9}$	$5.7\ 10^{-2}$	$6.3\ 10^{-2}$	post-shock cooling
21	2.00	1.80	2600	1.0	696	$3.0\ 10^{-11}$	$5.7\ 10^{-2}$	$6.3\ 10^{-2}$	variable κ_g

4.4. Influence of the stellar mass

Model No. 3 and Models No. 14–16 represent a series of calculations with varying stellar mass. As certainly to be expected an increase in stellar mass causes a reduction of the final outflow velocity but also an increase of the eigenperiod. In contrast, a reduction of the mass yields a shortening of the eigenperiod and an increase in the final outflow velocity. For this set of model parameters (2600K, $3\ 10^4\ L_\odot$, $\epsilon_C/\epsilon_O = 1.8$) no outflow is initiated for models above 1.6 $M_\star$. We conclude that the exterior κ–mechanism might only play a role for the mass loss of stars with low main sequence mass or for stars with higher main sequence mass that already have lost substantial amounts of mass on the AGB due to other mechanisms, e.g. the combined action of pulsation and radiation pressure on dust.

4.5. Influence of physical approximations

Model No. 17 has the same stellar parameters as Model No. 3 but is calculated without taking into account the dust opacity in the determination of the temperature in radiative equilibrium. As discussed in detail in Sect. 3.5 the neglect of the coupling between the dust complex and thermodynamics yields a stationary dust–driven wind solution for appropriately chosen stellar parameters.

In Tab. 2 Model No. 18 is labeled "stationary wind with shocks", a terminology which deserves some remarks. In fact, this model has been calculated without taking into account the dust opacity in the determination of the temperature in radiative equilibrium but with a piston applied at the inner boundary. The piston has a period of 650d and an amplitude of 2 km s^{-1}. The overall radial structure is similar, as one would expect, to the stationary dust–driven wind model presented in Sect. 3.5 and Fig. 6 (Model No. 17). However, the radial structure of the velocity is modulated by a periodic pattern of small–amplitude waves. For models of this kind pulsation is an additional feature which is not necessary to drive the wind. On the contrary, the support by pulsation yields unrealistic high mass loss rates and extremely high outflow velocities.

As indicated in Tab. 1, Model No. 19 is calculated with a piston at the inner boundary to simulate the interior pulsation. The piston again has an amplitude of 2 km s^{-1} and a period of 650d. Now the dust opacity *is* taken into account in the determination of the radiative equilibrium temperature. As discussed in detail in Sect. 3.3 and shown in Fig. 4 for high–luminosity models the piston only has minor influence on the resulting eigenperiod of the CDS. Even in the presence of a piston, the atmosphere still changes almost on the scale of its eigenperiod.

Table 2. Resulting quantities of the sample of model calculations to demonstrate the exterior κ–mechanism: mass loss rate $\dot{M}$, final outflow velocity u_∞, dust to gas ratio ρ_d/ρ_g, and eigenperiod. The parameter of the corresponding initial hydrostatic models are given in Tab. 1

	$<\dot{M}>$ [$M_\odot$ yr^{-1}]	$<u_\infty>$ [km s^{-1}]	ρ_d/ρ_g	Eigenperiod [650 d]	Remarks
1	2.7 10^{-5}	35.3	2.8 10^{-3}	1.4	
2	4.4 10^{-5}	26.0	1.7 10^{-3}	1.3	
3	1.8 10^{-5}	29.0	3.0 10^{-3}	1.7	
4	1.1 10^{-5}	28.3	2.6 10^{-3}	2.7	
5	2.7 10^{-7}	9.6	1.9 10^{-3}	3.2	
6	1.7 10^{-7}	5.8	6.4 10^{-4}	–	
7	2.3 10^{-5}	26.4	2.1 10^{-3}	1.9	
8	7.2 10^{-6}	17.7	1.0 10^{-3}	2.9	
9	3.4 10^{-7}	1.3	4.9 10^{-4}	>10	
10	–	–	–	–	no outflow
11	2.6 10^{-5}	34.4	3.3 10^{-3}	1.2	
12	1.2 10^{-7}	4.5	3.9 10^{-4}	>10	
13	3.6 10^{-9}	3.7	3.3 10^{-4}	>10	
14	2.0 10^{-5}	34.5	3.1 10^{-3}	1.1	
15	7.6 10^{-8}	9.0	4.8 10^{-4}	3.9	
16	2.0 10^{-8}	6.0	5.3 10^{-4}	>15	
17	1.7 10^{-5}	27.9	1.9 10^{-3}	–	stationary wind
18	2.4 10^{-3}	54.3	3.9 10^{-3}	–	stationary wind with shocks
19	4.6 10^{-5}	31.1	2.8 10^{-3}	1.4	
20	1.7 10^{-5}	34.1	2.6 10^{-3}	1.2	
21	5.6 10^{-8}	4.1	3.1 10^{-4}	>15	

The minor influence of the piston stems from the density gradient of these models in the innermost region. There, the models still have the initial density structure of the hydrostatic model, i.e. a less steep density gradient for the more luminous models. Therefore, the steepening of the dust–induced waves is confined to smaller amplitudes and the compression of the material is limited. Nevertheless, the densities are high enough to allow very effective growth without additional compression. Going to lower luminosities the input of additional energy, e.g. by pulsation, becomes more and more important. Then, the models are determined by the interaction of the two driving forces: the dust complex and the piston. Since the characteristic periods of these forces are different, the driving mechanisms might not interfere constructively. The whole system behaves like a forced pendulum, whose exterior force must not be in resonance with the eigenperiod of the pendulum.

By the preceding discussion, we get an idea how the effect of *multiperiodicity* (already mentioned in Papers I and II) occurs. If the ratio of the period of the piston and the eigenperiod of the atmosphere does not have an integer value n_P then the model behaves "irregularily" in the sense, that the radial structure of the dust shell does not reoccur after n_P pulsational cycles. If this ratio does take an integer value then we call the model a "regular" multiperiodic model, i.e. the radial structure of the model at a certain instant of time t_0 equals the radial structure at $t_1 = n_P P + t_0$, where P is the period of the piston. We call n_P the *multiperiodicity number*. That multiperiodicity also reflects in the lightcurves of the corresponding models has been demonstrated in Paper II.

For simplicity all models presented in Tab. 1 and 2 except No. 20 were calculated in the limit case of isothermal shocks. Taking into account LTE cooling of the gas behind the shocks causes only slight quantitative changes, but has no influence on the principal effect presented here.

However, significant quantitative changes occur if a variable gas opacity is taken into account, cf. Model No. 21. This fact is due to the differences which occur already in the initial hydrostatic model as described in Sect. 3.1. The considerable lower photospheric densities in models with variable gas opacity allow for only a less effective dust formation process, and hence, result in a prolonged eigenperiod and a substantially reduced outflow velocity. Nevertheless, if the luminosity is increased, e.g. to 3.0 10^4 $L_\odot$, the exterior κ–mechanism proceeds qualitatively as described in Sect. 3.2.

The mechanism presented in this paper is confirmed with a completely different numerical method by Höfner et al. (1994a), a detailed comparison between these two modeling approaches is discussed in Höfner et al. (1994b).

5. Conclusions

We have presented dynamical models of circumstellar dust shells around luminous carbon–rich long–period variables, which include time–dependent hydrodynamics and a detailed treatment of the processes of formation, growth and evaporation of dust grains. The models are calculated *without* using a piston at the inner boundary to simulate the interior pulsation of the star. Thus, the effect presented here is purely due to the behaviour of the CDS.

We have demonstrated that for sufficiently luminous models an instability in the CDS occurs, which causes these models to develop shock waves, even if *no* piston is applied at the inner boundary. We found that the dust opacity in the shell plays a central role in this process which therefore is called *exterior κ–mechanism*. Basically, this mechanism consists of the interaction of dust–induced small–amplitude waves and the processes of dust formation and growth.

It was demonstrated how the onset of this effect occurs in initially hydrostatic models. The stars under consideration are probably not in hydrostatic equilibrium, however. Small fluctuations are likely to be present in these objects, and could initiate the exterior κ–mechanism. Therefore, the effect should occur in stars with the appropriate stellar parameters. Since extremely high luminosities and low temperatures are needed for the mechanism to drive a stellar wind by itself, these conditions are only met during the very end of the AGB evolution.

For the appropriate parameters the exterior κ–mechanism is able to drive a massive slow outflow *without* the support of mechanical energy by the pulsation producing mass loss rates and terminal velocities typical for objects on the tip of the AGB. This finding supports the suggestion of e.g. Dominik et al. (1990) that purely dust–driven winds could provide a mechanism to account for the so–called "superwind" phase. The results demonstrate that dust–driven wind solutions indeed exist. However, our calculations revealed that taking into account all interactions leads to the development of instabilities. Thus, stationary dust–driven winds might only be a limiting case, and the "standard" solution shows a complicated internal structure and is highly time variable as discussed above.

The dynamics of the models, which show a pronounced exterior κ–mechanism, reveal an eigenperiod, which is the characteristic time scale between two dust–induced shocks. This eigenperiod was found to depend nonlinearly on the luminosity and to be inversely correlated with the overabundance of carbon to oxygen. If the piston is turned on at the inner boundary of these models with a period different from the eigenperiod, the behavior of very high–luminosity models remains unchanged since radiation pressure on dust grains completely dominates the dynamics of the shell.

In a broader range of parameters, i.e. for higher stellar temperatures and lower luminosities, the exterior κ–mechanism is not able to drive a wind by itself, but only with additional energy supply, e.g. by pulsation. The interaction between the time scale inherent to the CDS and the time scale introduced by the external force will then lead to the effect of multiperiodicity. Exemplary multiperiodic models have been already presented in Paper II.

Summarizing, the results again underline the importance of a detailed treatment of the formation of dust in *dynamical* models of LPVs. Taking into account the time dependence of the mechanisms reveals the nonlinear behaviour of the physical processes and leads to instabilities, a behaviour which is already known from the line–driven winds from hot stars. Thus, our finding somehow unifies the picture of mass loss mechanisms of giant stars.

Acknowledgements. We thank the referee, Dr. G. H. Bowen, for numerous comments and helpful suggestions that substantially improved the paper. AJF wants to thank J. M. Winters and S. Höfner for many fruitful discussions. The calculations were performed on the CRAY computers of the Konrad-Zuse-Zentrum für Informationstechnik Berlin and the HLRZ, Jülich. Subsequent data analysis has been performed on the WAP–cluster of the physics department of the TU–Berlin. This work has been supported by the Deutsche Forschungsgemeinschaft, *DFG*-Schwerpunkt "Theorie kosmischer Plasmen" (grant Se 420/5–3). Part of this research was performed under the auspices of the US Department of Energy.

References

Allen C.W., 1973, Astrophysical Quantities, The Athlone Press, London
Anders E., Zinner E., 1993, Meteoritics 28, 490
Berruyer N., Frisch H., 1983, A&A 126, 269
Bowen G.H., 1988, ApJ 329, 299
Bowen G.H., Willson L.A., ApJ 375, L53
Cadwell B.J., Wang H., Feigelson E.D., Frenklach M., 1994, ApJ 429, 285
Dominik C., Gail H.-P., Sedlmayr E., Winters J.M., 1990, A&A 240, 365
Donn B., Nuth J.A., 1985, ApJ 288, 187
Draine B.T., Salpeter E.E., 1977, J.Chem.Phys. 67, 2230
Feuchtinger M.U., Dorfi E.A., Höfner S., 1993, A&A 273, 513
Fleischer A.J., Gauger A., Sedlmayr E., 1991, A&A 242, L1
Fleischer A.J., Gauger A., Sedlmayr E., 1992, A&A 266, 321 (Paper I)
Gail H.-P., Sedlmayr E., 1985, A&A 148, 183
Gail H.-P., Sedlmayr E., 1987a, A&A 171, 197
Gail H.-P., Sedlmayr E., 1987b, A&A 177, 186
Gail H.-P., Sedlmayr E., 1988, A&A 206, 153
Gauger A., Gail H.-P. , Sedlmayr E., 1990, A&A 235, 345
Höfner S., Feuchtinger M., Dorfi E.A., 1994, A&A, in press
Höfner S., Fleischer A.J., Gauger A., Feuchtinger M., Dorfi E.A., Winters J.M., Sedlmayr E., 1994, A&A, in prep.

Hoffmeister C., Richter G., Wenzel W., 1984, Veränderliche Sterne, 2nd ed., Springer, Berlin
Jørgensen U.G., Johnson H.R., 1992, A&A 265, 168
Jura M., 1991, A&AR 2, 227
Knapp G.R., Morris M., 1985, ApJ 292, 640
Kozasa T., Hasegawa H., Seki J., 1984, Ap&SS 98, 61
Lambert D.L., Gustafsson B., Eriksson K., Hinkle K.H., 1986, ApJS 62, 373
Loup C., Forveille T., Omont A., Paul J.F., 1993, A&AS 99, 291
Lucy L.B., 1971, ApJ 163, 95
Lucy L.B., 1976, ApJ 205, 482
Maron M., 1990, Ap&SS 172, 21
Menietti J.D., Fix J.D., 1978, ApJ 224, 961
Olofsson H., Eriksson K., Gustafsson B., Carlström U., 1993a, A&AS 87, 267
Olofsson H., Eriksson K., Gustafsson B., Carlström U., 1993b, A&AS 87, 305
Ott U., 1993, Nature 364, 25
Owocki S.P., 1990, Rev. Mod. Astron. 3, 98
Owocki S.P., Castor J.I., Rybicki G.B., 1988, ApJ 335, 914
Pijpers F.P., 1994, A&A, in press
Richtmyer R.D., Morton K.W., 1967, Difference methods for initial-value problems, 2nd ed., John Wiley & Sons, New York
Rybicki, G.B., 1987, in: Instabilities in luminous early type stars, eds. H.J.G.L.M. Lamers and C.W.H. de Loore, Reidel, Dordrecht, p.175
Scholz M., Tsuji T., 1984, A&A 130, 11
Sedlmayr E., 1994, in: Molecules in the interstellar environment (IAU Coll. 146), ed. U.G. Jørgensen, Springer Verlag, Berlin, p.163
Sedlmayr E., Dominik C., 1994, Space Sci. Rev., in press
Tielens A.G.G.M., 1983, ApJ 271, 702
Winters J.M., Dominik C., Sedlmayr E., 1994a, A&A 288, 255
Winters J.M., Fleischer A.J., Gauger A., Sedlmayr E., 1994b, A&A, in press (Paper II)
Wood P.R., 1979, ApJ 227, 220

This article was processed by the author using Springer-Verlag LaTeX A&A style file *L-AA* version 3.